Available online at www.sciencedirect.com
ScienceDirect
Ceramics International 37 (2011) 1465–1471
CERAMICS INTERNATIONAL
www.elsevier.com/locate/ceramint

Turquoise blue nanocrystalline pigment based on $Li_{1.33}Ti_{1.66}O_4$: Synthesis and characterization

A. Fernández-Osorio [a,*], M.P. Jiménez-Segura [a], A. Vázquez-Olmos [b], R. Sato-Berru [b]

[a] Facultad de Estudios Superiores Cuautitlán, Universidad Nacional Autónoma de México A.P. 25, 54740 Edo de Méx., Mexico
[b] Centro de Ciencias Aplicadas y Desarrollo Tecnológico, Universidad Nacional Autónoma de México A.P. 70-186, 04510 México D.F., Mexico

Received 2 August 2010; received in revised form 8 September 2010; accepted 7 November 2010
Available online 2 December 2010

Abstract

Turquoise blue $Li_{1.33}Ti_{1.66}O_4$ is an environmentally friendly inorganic pigment, it was synthesized using the sol–gel method. The particle size was determined by X-ray diffraction (XRD) pattern and through high-resolution transmission electron microscopy (HRTEM), obtaining an average diameter of 27.5 ± 3 nm. The pigment shows a brilliant turquoise blue color, due to Ti^{3+}–Ti^{4+} intervalence charge transfer transitions and presents thermal stability up to 1000 °C. The $Li_{1.33}Ti_{1.66}O_4$ nanoparticles were characterized by using X-ray diffraction, Raman scattering and UV–vis absorption spectroscopy. The color properties and the thermal stability of this pigment suggest that it has potential to be applied as a satisfactory pigment for cosmetics, plastics, glasses and inks.

Keywords: A. Sol–gel process; C. Optical properties; Spinel pigments; Nanoparticles

1. Introduction

In the last years the study of spinel oxides nanostructured materials has attracted increasing interest due to its rich catalytic, color, electrical and magnetic properties. These materials are of special interest thanks to its improved properties such as lower temperature sinterability and great thermal stability [1–3].

Spinel oxides materials are also known to be very useful in the ceramic pigment industry. Inorganic pigments have been applied in various applications such as paints, ceramics, plastics, enamels, and glasses [4], however, most of the conventional inorganic pigments applicable for the above applications contain toxic elements such as Cd, Co, Cr, Hg, Pb, Sb and Se, that can adversely affect environmental and human health. Therefore, development of safe inorganic pigments has been required in order to replace toxic inorganic pigments [5]. The most straightforward way to obtain blue colors in ceramics is by means of cobalt, which has been used since antiquity [6]. Available industrial blue pigments are Co_2SiO_4, $CoAl_2O_4$, vanadium doped zircon V-$ZrSiO_4$ [7–10] and the turquoise blue pigments of Ni doped $CaAl_{12}O_{19}$ reported by Costa et al. [11].

In this way, turquoise blue $Li_{1.33}Ti_{1.66}O_4$ is an environmentally friendly inorganic pigment that can be applied to glass, plastics, paints, cosmetics and inks. In the family of oxide spinels only the $Li_{1+x}Ti_{2-x}O_4$ ($0 \leq x \leq 1/3$) solid solution series become superconducting, while $LiTi_2O_4$ is metal-like with a superconducting transition temperature of 12.7 K, the end member $Li_{4/3}Ti_{5/3}O_4$ is a good insulator with rather high resistivity [12,13]. This solid solution was originally synthesized and structurally characterized by Deschanvres et al. [14]. Research in the late 1970s and early 1980s was focused on the development of lithium oxide spinel electrodes for rechargeable lithium batteries [15].

The general formula for the normal spinel structure is AB_2O_4, where A refers to cations in the tetrahedral sites and B represents the cations in octahedral positions in a cubic geometry with symmetry Fd3m [16]. The normal structure presents the $A(B_2)O_4$ distribution and the inverse one the $B(AB)O_4$, in both cases the parentheses represent the octahedral positions. In fact, there are many possible intermediary cation distributions. This complicated crystallographic structure, has a unique perspective for studies of substitution and their relationships with the chemical and

* Corresponding author. Tel.: +52 55 5623 2007; fax: +52 55 5623 1887.
E-mail address: ana8485@8485servidor.unam.mx (A. Fernández-Osorio).

0272-8842/$36.00
doi:10.1016/j.ceramint.2010.11.015

physical properties [17,18]. For $Li_{1.33}Ti_{1.66}O_4$ in particular, Ti^{3+} and Ti^{4+} ions occupy the octahedral sites, Li^{1+} ions occupy the tetrahedral sites, and the additional Li^{1+} ions also occupy octahedral sites [19–21]. The crystalline structure can be determined by the XRD pattern because of the difference in atomic scattering factors between titanium and lithium ions [22,23].

Titanium is predominantly a tetravalent ion on Earth, whereas the relatively unstable Ti^{3+} ions are more abundant in extraterrestrial minerals, Moon rocks and some meteorites. The $3d^1$ configuration of Ti^{3+} ions octahedrally coordinated results in a ground-state $(t_{1g})^1$ $(e_g)^0$ and an excited state $(t_{2g})^0$ $(e_g)^1$, configurations represented by $^2T_{2g}$ and ^2E_g crystal field states, respectively. Therefore, one spin-allowed crystal field band ($^2T_{2g} \rightarrow {}^2E_g$ transition) is expected in optical spectra [24].

In general, the synthesis of wide ranges of bulk lithium titanium oxides involves wet chemical techniques such as co-precipitation, sol–gel, hydrothermal; solid state reaction and Pechini process [25,26].

In this work, the sol–gel route based on the modified Pechini method was employed to obtain turquoise blue $Li_{1.33}Ti_{1.66}O_4$ nanocrystalline. The polymeric precursor method reduces individualities of different metal ions, which can be achieved by encircling stable metal complexes with growing polymer nets. The immobilization of metal complexes in such rigid organic polymeric networks can reduce the segregation of particular metals, thus ensuring compositional homogeneity on a molecular scale. This method is specially useful for stoichiometric composition control [27,28].

2. Experimental procedure

2.1. Sample preparation

$Li_{1.33}Ti_{1.66}O_4$ pigment was synthesized as follows: 2.4488 g of lithium acetate dihydrate ($C_3H_3O_2Li{\cdot}2H_2O$) (99.8% Sigma–Aldrich) was dissolved in 20 ml of 2-metoxyethanol $CH_3O(CH_2)_2OH$ (99.9% Sigma–Aldrich) stirring for 30 min, 7.1172 g of titanium (IV) isopropoxide $Ti(OCH(CH_3)_2)_4$ (99.8% Aldrich) were then added to this solution. Afterwards, 5 ml of ultra-pure water (ultra-pure water (18 MΩ) obtained from Barnstead E-pure deionization system) were added, obtaining a white gel.

This gel was dried at room temperature for five days and, when it was completely dry, it was ground in agate mortar and annealed in air for 2 h at 200 °C, 300 °C, 400 °C, 500 °C, 600 °C, 700 °C and 800 °C, respectively. After each annealing, the sample was analyzed with X-ray powder diffraction.

The polymeric gel has been obtained from the reaction of lithium acetate with titanium alkoxide, a fraction of Ti^{4+} ions are reduced to Ti^{3+} because lithium hydroxide is a valuable reducing agent in organic synthesis. The formulas of the polymeric gels are found from chemical analysis and can be confirmed by IR and NMR spectroscopies [29]. Fig. 1 shows a reaction scheme proposed.

In order to compare the sol–gel method with another typical procedure for obtaining these pigments, we follow a conventional solid-state reaction method (the ceramic route), to prepare a batch composition of TiO_2–Ti_2O_3–$LiNO_3$ system (Table 1). The mixtures were calcined in an electric kiln at 800 °C for 2 h.

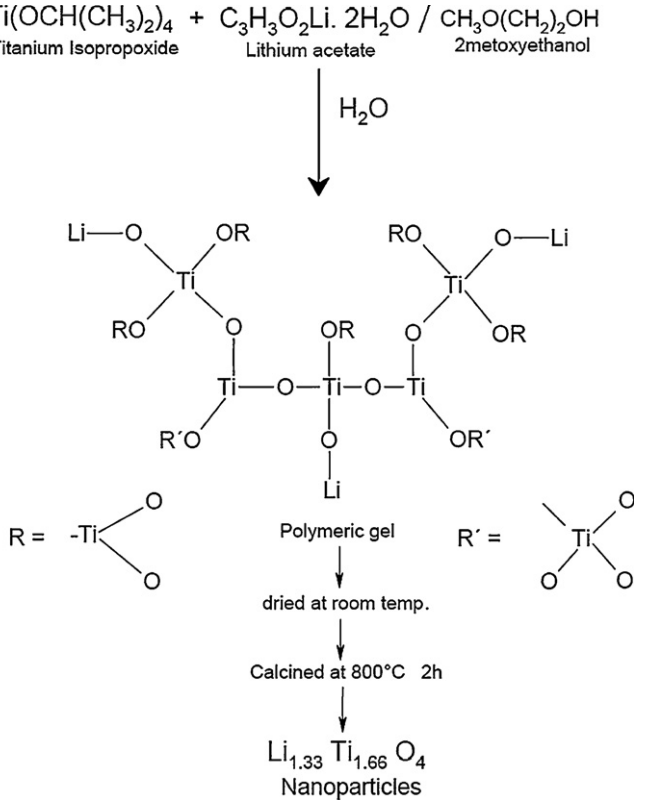

Fig. 1. Proposed reaction scheme for obtaining $Li_{1.33}Ti_{1.66}O_4$ nanoparticles.

2.2. Experimental techniques

X-ray diffraction patterns of the samples were recorded at room temperature with Cu Kα radiation in a D5000 Siemens diffractometer. Intensity was measured in the 2θ range between 2.5° and 70°. The average crystallite size was approximately estimated by the Scherrer's equation using the full width at half maximum (FWHM) of the most intense peaks. As reported in the literature [30] the Scherrer's equation is described as follows:

$D = 0.9\lambda/B \cos\theta$, where λ is the wavelength of Cu Kα (1.54056 Å), θ is the angle of Bragg diffraction and B is the FWHM, without using any material for the estimation of instrumental broadening.

Table 1
Prepared pigment formulations.

Reference	Composition	TiO_2	Ti_2O_3	$LiNO_3$	Atmosphere
	Molar ratio	1.66		1.5	
2Li–Ti	wt (%)	56.7		43.2	Air
3Li–Ti	wt (%)	56.7		43.2	Argon
	Molar ratio	0.83	0.41	1.5	
4Li–Ti	wt (%)	28.9	25.9	45.1	Air

Raman spectra were obtained from 200 to 12 000 cm^{-1} with a Nicolet Almega XR dispersive Raman spectrometer, using a scan time of 25 s and a resolution of ~4 cm^{-1}. An Nd: YVO_4 532-nm laser was used for excitation and the incident power on the sample was ~10 mW.

The UV–vis electronic absorption spectra of the powdered samples were performed by diffuse reflectance technique, in an Ocean Optics HR4000 spectrometer equipped with an Integrating Sphere for reflectance, the powders are pressed against the sample port of the Integrating Sphere using $BaSO_4$ as a reference.

The color properties of the sample were estimated by measuring the CIE *L* a* b** parameters using diffuse reflectance spectroscopy data in the visible range.

High-resolution transmission electron microphotographs (HR-TEM) were obtained in a JEOL 2010 FasTEM analytical microscope, operating at 200 kV, by deposition of a drop of the powdered transition metal oxide dispersed in N,N′-dimethyl-formamide (DMF) onto 300 mesh Cu grids coated with a carbon layer.

3. Results and discussion

3.1. Phase composition and crystal structure

Fig. 2 illustrates the XRD patterns for the dried polymeric gel calcined at various reaction temperatures, from 100 to 800 °C.

The XRD patterns of the sample sintered at 400 and 500 °C show the TiO_2 anatase phase, while the samples annealed at temperatures higher than 500 °C the anatase phase was transformed into the rutile phase and also displays the diffraction peaks characteristics of $Li_{1.33}Ti_{1.66}O_4$ compound. Finally, when the sample was heated up to 800 °C, $Li_{1.33}Ti_{1.66}O_4$ nanocrystalline turquoise blue pigment corresponding to a single spinel phase, was obtained (Fig. 3). This sample was named 1Li–Ti.

In its corresponding XRD pattern all peaks can be perfectly indexed to the crystalline $Li_{1.33}Ti_{1.66}O_4$ (JCPDS 26-1198) with Fd3m space group, and a cell parameter of 8.357 Å. The observed broad hump in the 15–35° range, implies the occurrence of an amorphous phase in the sample due to residual organic impurities of the polymeric gel decomposition.

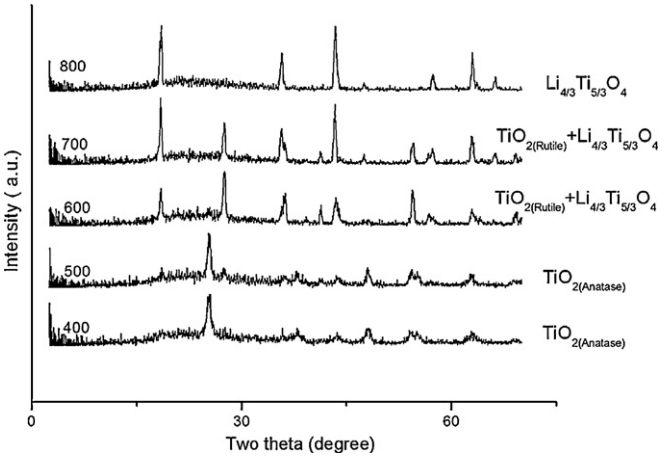

Fig. 2. X-ray diffraction patterns of the sample prepared by sol–gel heated at temperatures between 400 and 800°C.

In order to determine the average crystallite size, a peak broadening method was applied using the Scherrer's equation over (1 1 1), (3 1 1) and (4 0 0) reflections, finding it to be of 29.3, 33.5 and 19.8 nm, respectively.

3.2. Thermal stability

In order to study the thermal stability of $Li_{1.33}Ti_{1.66}O_4$ nanocrystalline compound prepared by the sol–gel method (1Li–Ti), it was heated in air for 2 h at 800 °C, 900 °C and 1000 °C, respectively. After each annealing, the sample was analyzed with X-ray powder diffraction. Fig. 4 shows their corresponding X-ray diffraction patterns.

This phase (1Li–Ti) remains stable even after annealing the sample at 1000 °C, but it decomposes at 1014 °C into Li_2TiO_3 and $Li_2Ti_3O_7$ solid phases.

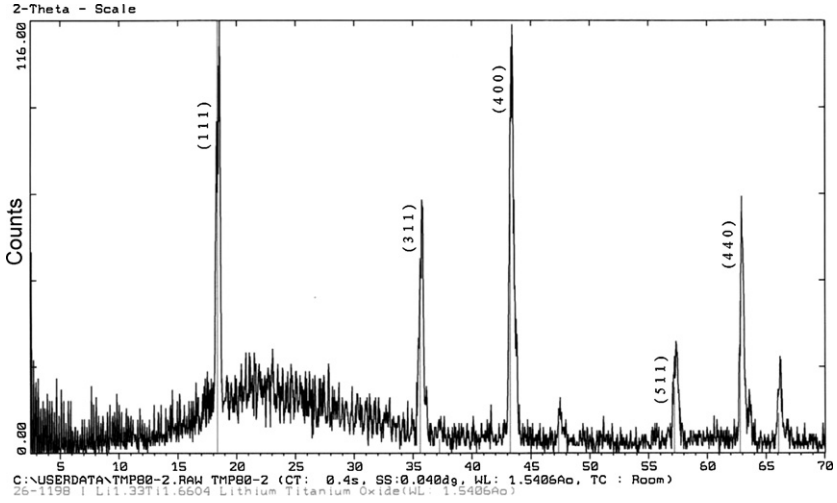

Fig. 3. X-ray diffraction pattern of the sample prepared by sol–gel heated 800°C/2 h.

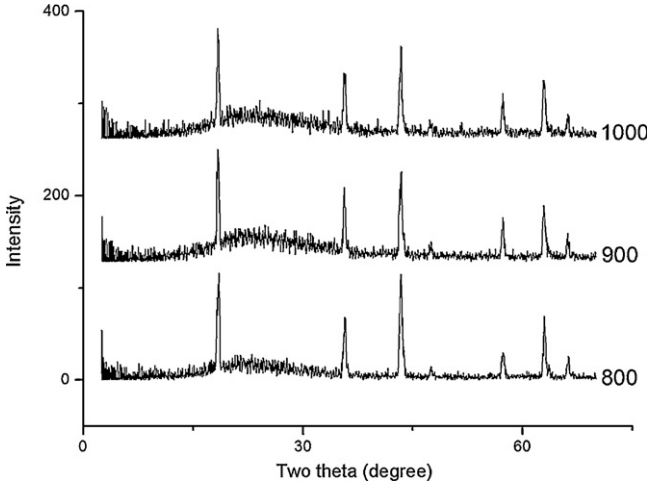

Fig. 4. X-ray diffraction patterns of $Li_{1.33}Ti_{1.66}O_4$ prepared by sol–gel heated for 2 h at temperatures of 800, 900 and 1000° C.

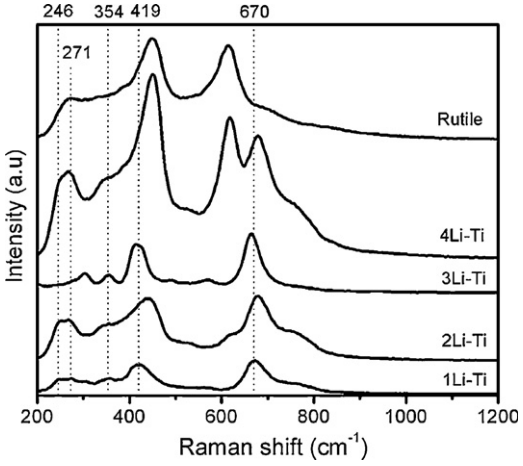

Fig. 6. Raman spectra of $Li_{1.33}Ti_{1.66}O_4$prepared by sol–gel and the ceramic method.

Fig. 5, meanwhile, shows the corresponding XRD patterns of 2Li–Ti, 3Li–Ti and 4Li–Ti samples, prepared using the conventional ceramic route.

2Li–Ti and 3Li–Ti samples are identified as single phase of $Li_{1.33}Ti_{1.66}O_4$ while 4Li–Ti is a powder corresponding to $Li_{1.33}Ti_{1.66}O_4$ and TiO_2 (rutile) phases.

The sample 4Li–Ti was prepared by heating TiO_2, Ti_2O_3 and $LiNO_3$ powders. In the X-ray diffraction patterns of this sample, peaks of $Li_{1.33}Ti_{1.66}O_4$ began to appear at 700 °C increased in height with increasing temperature from 700 to 800 °C whereas those of Ti_2O_3 and $LiNO_3$ decreased, in the X-ray diffraction pattern of the powder obtained at 800 °C, $Li_{1.33}Ti_{1.66}O_4$ was the main phase with a small amount of TiO_2 and no Ti_2O_3 and $LiNO_3$ were detected. We expect with a temperature above 800 °C, the TiO_2 phase will disappear, and a single phase of $Li_{1.33}Ti_{1.66}O_4$ will be obtained.

3.3. Raman spectroscopy

It is commonly accepted that normal AB_2O_4 spinel exhibits a cubic structure with space group Fd3m with $Z = 8$. Cations occupy only 1/8 of the tetrahedrally coordinated sites (8a Wyckoff position) and 1/2 of the octahedrally coordinated sites (16d Wyckoff position), A atoms are located on tetrahedral sites of T_d symmetry and B atoms on octahedral sites of $D_3{}^d$ symmetry, whereas oxygen atoms occupy C_3 sites (32e Wyckoff position).

In spinel lithium titanium oxides for a regular octahedral $TiO_6{}^{2-}$ with O_h symmetry, three stretching modes ν_1 (A_{1g}), ν_2 (E_g) and ν_3(F_{1u}) and three bending modes ν_4(F_{1u}), ν_5(F_{2g}) and ν_6(F_{2u}) are allowed, where ν_1, ν_2, and ν_3 are Raman-active modes, ν_3 and ν_4 are infrared active modes and ν_6 is a silent mode. The assignment of modes observed in the Raman spectrum of $Li_{1+x}Ti_{2-x}O_4$ has been reported previously [31].

Fig. 6 shows the Raman spectra of 1Li–Ti, 2Li–Ti, 3Li–Ti and 4Li–Ti in the spectral region between 200 and 900 cm^{-1}.

A common feature of these spectra is the presence of a strong band around 670 cm^{-1} and a group of bands between 200 and 500 cm^{-1} with weaker intensity. In spinel oxides and in other titanium oxides, energies of ≈600–670 cm^{-1} are characteristic of vibrations involving the motion of oxygen atoms inside the octahedral unit TiO_6 [32]. The Raman band located at about 670 cm^{-1} is viewed as the symmetric Ti–O stretching vibration of TiO_6 groups. This high-wave number is assigned to the A_{1g} species in the $O_h{}^7$ spectroscopic symmetry. Its broadness is related to the cation–anion bond lengths and polyhedral distortion occurring in $Li_{1+x}Ti_{2-x}O_4$. As the titanium ion of the spinel structure exhibits a charge disproportionation such as Li ($Ti^{3+}Ti^{4+}$) O_4, there are isotropic $Ti^{4+}O_6$ octahedra and locally distorted $Ti^{3+}O_6$ octahedra due to the Jahn Teller effect. Thus we expect to observe stretching vibration of $TiO_6{}^{9-}$ and $TiO_6{}^{8-}$ octahedral which provides the broadness of the A_{1g} mode.

The RS peak with medium intensity located a 419 cm^{-1} has the $F_{2g}{}^{(2)}$ symmetry, while the weak bands located at 354 and 271 cm^{-1} have the E_g and $F_{2g}{}^{(3)}$ symmetry, respectively. The $F_{2g}{}^{(3)}$ mode is related to the Li–O motion, connected to the tetrahedral cation movements. The low-wavenumber band at 300 cm^{-1} which appears in 3Li–Ti is a unexpected mode, which could be Raman-active due to the cationic disorder.

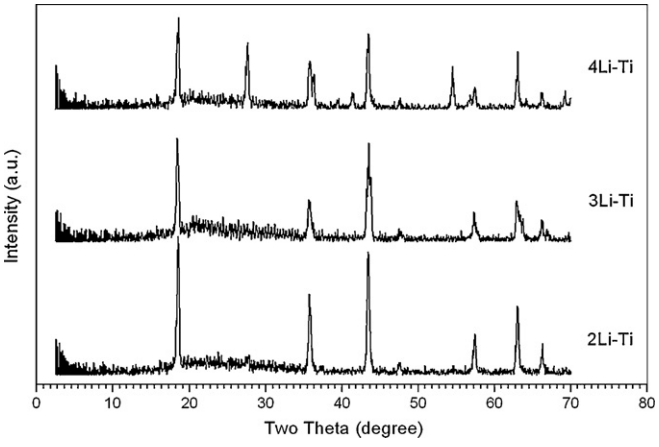

Fig. 5. XRD patterns of the samples prepared using the ceramic route.

It can be stated that in the cubic spinel Li Ti_2O_4 the Ti^{3+} and Ti^{4+} ions are considered as crystallographically equivalent (16d sites) in agreement with XRD data, therefore, occupation probabilities of 0.5 must be affected for each cation in the 16d position. Hence, a loss of translation invariance certainly occurs due to local lattice distortion around the Ti^{3+} cations which exhibit a JT effect [33].

As the series of spinel-type lithium titanium oxides $Li_{1+x}Ti_{2-x}O_4$, or $(Li)_{tetr}$ $[Li_xTi_{2-x}]_{oct}$ O_4 in spinel notation, and for 1Li–Ti, Li $[Li_{0.33}Ti^{3+}{}_{0.83}Ti^{4+}{}_{0.83}]$ O_4 contain Li ions in vacant 16d octahedral sites, and Ti^{3+} ions exhibit JT effect we can expect a slight tetragonal distortion, however according to the XRD pattern, presents cubic spinel structure. Furthermore, this would be consistent with the fact that the spectral features in the RS spectra of $Li_{1.33}Ti_{1.66}$ O_4 (1Li–Ti, 2Li–Ti, 3Li–Ti) are not markedly different from those of $LiTi_2O_4$, where a significant increase of the peak located at 354 cm^{-1} occurs.

It was speculated that this Raman band is partly related to the stretching vibration of Li ions in octahedral coordination [34]. The 4Li–Ti sample also displays rutile peaks.

3.4. UV–vis absorption spectroscopy

The UV–vis diffuse reflectance spectra of the samples 1Li–Ti, 2Li–Ti and 3Li–Ti are shown in Fig. 7.

1Li–Ti presents a broad absorption band between 550 and 750 nm, in this range there are three bands at 580, 610 and 660 nm.

The spectrum of 1Li–Ti ($Li_{1.33}Ti_{1.66}O_4$) in addition to possessing Ti^{3+} crystal bands at 580 and 610 nm assigned to dynamic Jahn Teller splitting of the ^2E_g level or the occurrence of Ti^{3+} ions in distorted octahedral sites, contains a $Ti^{3+} \rightarrow Ti^{4+}$ intervalence band centered near 660 nm involving adjacent Ti^{3+} and Ti^{4+} cations in edge-shared octahedral sites in the spinel structure.

Absorption spectra of synthetic Ti^{3+} doped Al_2O_3 crystals show two spin allowed crystal field bands occurring at

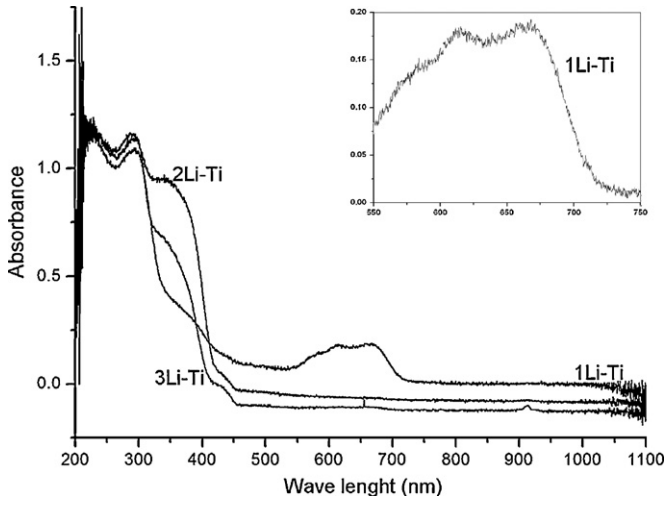

Fig. 7. UV–vis spectra of $Li_{1.33}Ti_{1.66}O_4$prepared by sol–gel (1Li–Ti) and by the ceramic route (2Li–Ti and 3Li–Ti).

18 450 cm^{-1} and 20 300 cm^{-1}. These originate from Ti^{3+} ions in the trigonally distorted, symmetry C_3, octahedral site of the corundum structure. Absorption bands at similar energies also occur in optical spectra of blue sapphire [35], it is Al_2O_3 with traces of Fe^{2+}, Fe^{3+}, Ti^{3+}, Ti^{4+}, when Fe^{2+} and Ti^{4+} ions occupy two adjacent sites in a corundum crystal, the transfer of an electron occur:

$$Fe^{2+} + Ti^{4+} \rightarrow Fe^{3+} + Ti^{3+}$$

Intervalence charge transfer is a process that produces a strong colored appearance at a low percentage of transition metal cations.

The green clinopyroxene, is particularly interesting because it is devoid of iron and contains coexisting Ti^{3+} and Ti^{4+} ions. The spectra of this pyroxene, Ca (Mg, Ti^{3+}, Ti^{4+}, Al) (Si, $Al)_2O_6$, shows two well defined bands around 16 000 cm^{-1} and 20 000 cm^{-1} assigned to crystal field transitions in Ti^{3+} ions located in the distorted octahedral site, and an additional inflexion around 15 000 cm^{-1} assignment as $Ti^{3+} \rightarrow Ti^{4+}$ intervalence charge transfer, involving adjacent Ti cations separated by 315 pm in edge-shared octahedral sites in the pyroxene structure [36].

By analogy with the $Fe^{2+} \rightarrow Fe^{3+}$ charge transfer band in vivianite, the energy of this pyroxene $Ti^{3+} \rightarrow Ti^{4+}$ charge transfer bands have been identified in a number of synthetic Ti compounds; the weak broad band around 12 500 cm^{-1} in the spectra of Ti^{3+} doped Al_2O_3 crystals may also originate from electron transfer between Ti cations only 269 pm or 297 pm apart in face shared or edge shared octahedral of the corundum structure [37]. Coexisting Ti^{3+} and Ti^{4+} ions frequently, suggesting that charge transfer transition may occur between the cations when they are situated in adjacent coordination sites in the crystal structure [38].

However, 2Li–Ti and 3Li–Ti do not present absorption bands in the visible range of the electromagnetic spectrum (Fig. 6). They are white powders, because we think Ti^{3+} and Ti^{4+} do not occupy adjacent octahedral sites in the spinel structure, cation disorder is present in octahedral sites.

The local order in the sample prepared using the sol–gel method (1Li–Ti) is described by representative octahedra, made of oxygen ions in its vertices and titanium ions near the center, arranged alternatively (Ti^{3+}, Ti^{4+}). The long-range order is given by the way these octahedra interact between each other [38]. There is an interaction between these octahedra, allowing a $Ti^{3+} \rightarrow Ti^{4+}$ intervalence band, responsible for the color in this pigment.

The color turquoise is achieved in the 1Li–Ti sample, as shown by the negative values for the chromatic parameters b^* (blue) and a^* (green), as well as the L^* (brightness). 1Li–Ti exhibits the color turquoise blue with a blue component ($b^* = -3.8$), greener ($a^* = -13$) and brightness $L^* = 95.8$.

The HR-TEM micrograph (Fig. 8) shows an isolated $Li_{1.33}Ti_{1.66}O_4$ nanocrystallite with dimensions of about 20.5 nm. The interplanar distances determined from their corresponding electron diffraction patterns confirm that the nanocrystals are composed of $L_{1.33}Ti_{1.66}O_4$.

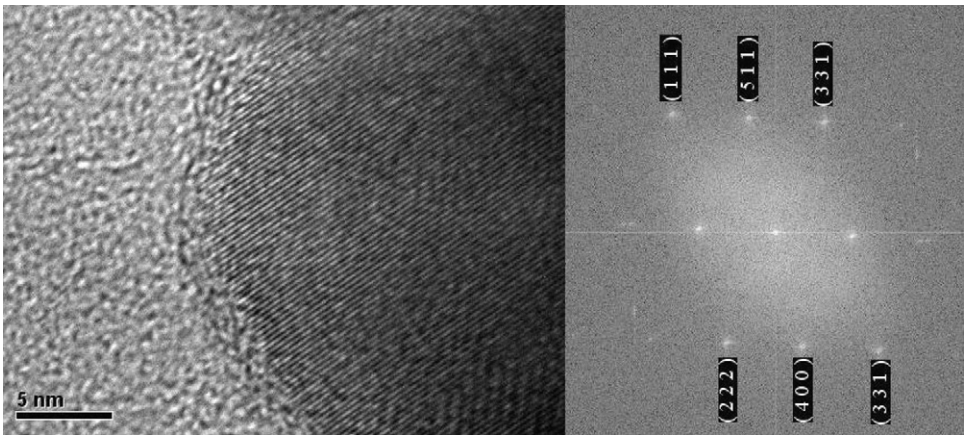

Fig. 8. HRTEM of 1Li–Ti (prepared by the sol–gel method).

4. Conclusions

Nanocrystalline $Li_{1.33}Ti_{1.66}O_4$ was synthesized using two different methods: sol–gel and the ceramics route. The color developed in this pigment depends on the synthesis route. The sol–gel method, with titanium alkoxide and lithium acetate dihydrate as precursors, allows the development of a local order in the crystalline structure, generating a turquoise blue color. This method produces crystalline material of $Li_{1.33}Ti_{1.66}O_4$. The optical properties and thermal stability of this pigment suggest that this material has the potential to be applied as an environmentally friendly coloring agent for cosmetics, glasses, plastics and inks.

Acknowledgement

The support of this research by the UNAM-PAPIME project PE100509 is gratefully acknowledged.

References

[1] P.M.T. Cavalcante, M. Dondi, G. Guarini, M. Raimondo, G. Balde, Colour performance of ceramic nano-pigments, Dyes Pigments 80 (2009) 226–232.
[2] M. Cain, R. Morrell, Nanostructured ceramics: a review of their potential, J. Organomet. Chem. 15 (2001) 321–330.
[3] X. Wei, D. Chen, Synthesis and characterization of nanosized zinc aluminate spinel by sol–gel technique, Mater. Lett. 60 (2006) 823–827.
[4] H.M. Smith, High Performance Pigments, Wiley/VCH, Weinheim, 2002.
[5] S. Furokawa, T. Masui, N. Imanaka, Synthesis of new environment friendly yellow pigments, J. Alloys Compd. 418 (2006) 255–258.
[6] R. Eppler, D. Eppler, Glazes and Glass Coating, The American Ceramic Society, Westerville, Ohio, 2000.
[7] M. Llusar, A. Forés, J.A. Badenes, J. Calb, M.A. Tena, G. Monrós, Colour analysis of some cobalt-based blue pigments, J. Eur. Ceram. Soc. 21 (2001) 1121–1130.
[8] C. Caselli, G. Lusvardi, G. Malavasi, L. Menabue, P. Miselli, Multi-technique approach to V-$ZrSiO_4$ pigment characterization and synthesis optimization, J. Eur. Ceram. Soc. 27 (2007) 1743–1750.
[9] S. Ardizzone, Structural and spectroscopic investigations of blue, vanadium doped $ZrSiO_4$ pigments prepared by a sol–gel route, J. Phys. Chem. B 109 (2005) 22112–22119.
[10] A. Forés, M. Llusar, J.A. Badenes, J. Calbo, M. Tena, G. Monrós, Alternative turquoise blue pigment for glazes, Am. Ceram. Soc. Bull. 80 (2001) 47–52.
[11] G. Costa, M.J. Ribeiro, W. Hajjaji, M.P. Seabra, J.A. Labrincha, M. Dondi, G. Cruciani, Ni-doped hibonite ($CaAl_{12}O_{19}$): a new turquoise blue ceramic pigment, J. Eur. Ceram. Soc. 29 (2009) 2671–2678.
[12] X.G. Qiu, C.Z. Bi, J.Y. Ma, X. Fang, M. Kamran, B.R. Zhao, Superconducting properties of spinel $Li_{1+x}Ti_{2-x}O_4$ and their substitution effects, Physica C 462 (2007) 540–543.
[13] D.C. Johanston, H. Prakash, W.H. Zachariesen, R. Viswanathan, High temperature superconductivity in the Li–Ti–O ternary system, Mater. Res. Bull. 8 (1973) 777–784.
[14] A. Deschanvres, B. Raveau, Z. Sekkal, Mise en evidence et etude cryystallographique dúne novelle solution solide de type spinelle Li_{1+x}-$Ti_{2-x}O_4$, Mater. Res. Bull. 6 (1971) 699–705.
[15] M.M. Thackeray, Spinel electrodes for lithium batteries, J. Am. Ceram. Soc. 82 (1999) 3347–3354.
[16] H. O'Neill, A. Navrotsky, Simple spinels: crystallographic parameters, cation radii, lattice energies and cation distribution, Am. Mineral. 68 (1983) 181–194.
[17] K.E. Sickafus, J.M. Willis, N.W. Grimes, Structure of spinel, J. Am. Ceram. Soc. 82 (1999) 3279–3286.
[18] A.N. Cormack, G.V. Lewis, S.C. Parker, C.R. Catlow, On the cation distribution of spinels, J. Phys. Chem. Solids 49 (1988) 53–57.
[19] S. Takai, M. Kamata, S. Fujine, K. Yoneda, K. Kanda, T. Esaka, Diffusion coefficient measurement of lithium ion in sintered $Li_{1.33}Ti_{1.66}O_4$ by means of neutron radiography, Solid State Ionics 72 (1999) 165–172.
[20] C. Chen, M. Spears, F. Wondre, J. Ryan, Crystal growth and superconductivity of $LiTi_2O_4$ and $Li_{1+1/3}$ $Ti_{2-1/3}O_4$, J. Cryst. Growth 250 (2003) 139–145.
[21] D. Fattakhova, V. Petrykin, J. Brus, T. Kostlanova, J. Dedecek, P. Krtil, Solvothermal synthesis and electrochemical behavior of nanocrystalline cubic Li–Ti–O oxides with cationic disorder, Solid State Ionics 176 (2005) 1877–1885.
[22] G.X. Wang, D.H. Bradhurst, S.X. Dou, H.K. Liu, Spinel $Li[Li_{1/3}Ti_{5/3}]O_4$ as an anode material for lithium batteries, J. Power Sources 83 (1999) 156–161.
[23] Y. Takahashi, Y. Gotoh, J. Akimoto, Structure and electron density analysis of oxide spinel $LiTi_2O_4$, J. Phys. Chem. Solids 63 (2002) 987–990.
[24] R.G. Burns, Mineralogical Applications of Crystal Field Theory, second ed., Cambridge University Press, Cambridge, 1993.
[25] C.Q. Feng, L. Li, Z.P. Guo, D.Q. Shi, R. Zeng, X.J. Zhu, Synthesis and properties of Li–Ti–O spinel ($LiTi_2O_4$), J. Alloys. Compd. 478 (2009) 767–770.
[26] E.C. Paris, E.R. Leite, E. Longo, J.A. Varela, Synthesis of $PbTiO_3$ by use of polymeric precursors, Mater. Lett. 37 (1998) 1–5.
[27] J. Livage, The gel route to transition metal oxides, J. Solid State Chem. 64 (1986) 322–330.
[28] M.S.C. Camara, P.N. Lisboa-Filho, M.D. Cabrelon, L. Gama, W.A. Ortiz, C.O. Paiva-Santos, E.R. Leite, E. Longo, Synthesis and characterization of $Li_2ZnTi_3O_8$ spinel using the modified polymeric precursor method, Mater. Chem. Phys. 82 (2003) 68–72.

[29] F. Babonneau, C. Sanchez, J. Livage, Spectroscopic characterization of sol–gel processing, J. Non-Cryst. Solids 106 (1988) 170–173.
[30] A.L. Patterson, The Scherrer formula for X-ray particle size determination, Phys. Rev. 56 (1939) 978–982.
[31] D.Z. Liu, W. Hayes, M. Kurmoo, M. Dalton, C. Chen, Raman scattering of the $Li_{1+x}Ti_{2-x}O_4$superconducting system, Phys. C: Superconductivity (1994) 235–240.
[32] K. Mukai, K. Ariyoshi, T. Ohzuku, Comparative study of $Li[CrTi]O_4$, $Li[Li_{1/3}Ti_{5/3}]O_4$ and $Li_{1/2}Fe_{1/2}[Li_{1/2}Fe_{1/2}Ti]O_4$ in non-aqueous lithium cells, J. Power Sources 146 (2005) 213–216.
[33] A.B.P. Lever, Inorganic Electronic Spectroscopy, second ed., Elsevier, Amsterdam, 1984.
[34] C.M. Julien, M. Massot, Raman spectroscopic studies of lithium manganates with spinel structures, J. Phys.: Condens. Matter 15 (2003) 3151–3162.
[35] M. Kadleikova, J. Breza, M. Vasely, Raman spectra of synthetic sapphire, Microelectron. J. 32 (2001) 955–959.
[36] G.R. Rossman, Reviews in Mineralogy: Piroxenes, vol. 7, Mineralogical Society of America, 1980 (Chapter 3).
[37] R.G Burns, Mineralogical Applications of Crystal Field Theory, second ed., Cambridge University Press, Cambridge, 1993.
[38] X. Bokhimi, A. Morales, M. Aguilar, J.A. Toledo-Antonio, F. Pedraza, Local order in titania polymorphs, Int. J. Hydrogen Energy 26 (2001) 1279–1287.